Single-Molecule Spectroscopy Using Microfluidic Platforms

ARTICLE *in* METHODS IN ENZYMOLOGY · JANUARY 2010

Impact Factor: 2.09 · DOI: 10.1016/S0076-6879(10)72013-9 · Source: PubMed

2 AUTHORS:

Samuel kim Kim
Auckland University of Tech…
40 PUBLICATIONS **648**
CITATIONS

SEE PROFILE

Richard Zare
Stanford University
1,151 PUBLICATIONS **44,218**
CITATIONS

SEE PROFILE

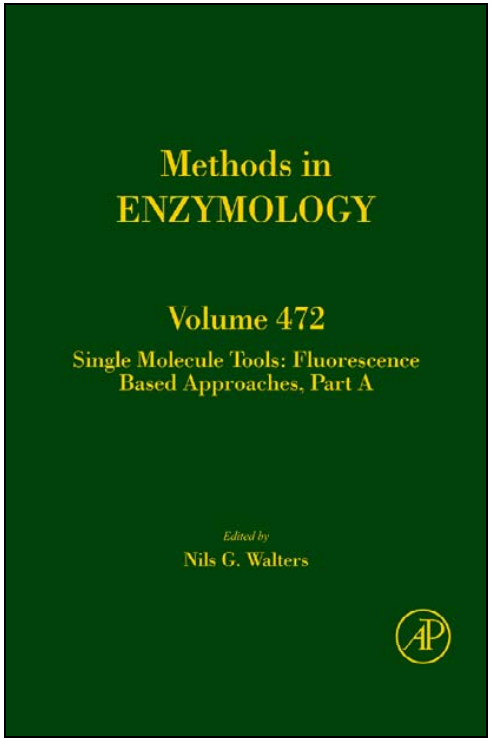

From: Samuel Kim1 and Richard N. Zare, Single-Molecule Spectroscopy Using Microfluidic Platforms
In Nils G. Walters editor: *METHODS IN ENZYMOLOGY,* Vol. 472,
Burlington: Academic Press, 2010, pp.119-132.
ISBN: 978-0-12-374954-3

CHAPTER SEVEN

Single-Molecule Spectroscopy Using Microfluidic Platforms

Samuel Kim[1] *and* Richard N. Zare

Contents

Abstract

Microfluidics serves as a convenient platform for single-molecule experiments by providing manipulation of small amounts of liquids and micron-sized particles. An adapted version of capillary electrophoresis (CE) on a microchip can be utilized to separate chemical species with high resolution based on their ionic mobilities (i.e., charges and sizes), but identification of separated species is not trivial, especially for complex mixtures of sticky biomolecules. We describe here how to use a surfactant mixture system for CE on a poly(dimethylsiloxane) (PDMS) microchip, capture separated peaks within a 50-pl chamber using microvalves, analyze the fluorescence signals with correlation spectroscopy to extract molecular diffusion characteristics, and to identify the biomolecular clusters in a model immunocomplex system.

Department of Chemistry, Stanford University, Stanford, California, USA
[1] Current address: Polymer Research Institute and National Core Research Center for Systems Bio-Dynamics, Pohang University of Science and Technology, Pohang, Kyungbuk, South Korea

Methods in Enzymology, Volume 472
ISSN 0076-6879, DOI: 10.1016/S0076-6879(10)72013-9

1. Introduction

Microfluidics refers to the study and control of the fluidic behavior of a liquid within structures of micrometer dimensions. Because of its ability to handle extremely small amounts of samples and microscale objects such as cells, the use of the technique in various types of single-molecule experiments has rapidly increased. For instance, microfluidic channels were used to prepare compartmentalized neuron cell cultures for single-particle tracking of nerve growth factor molecules (Cui *et al.*, 2007). Single-cell expression assay of β-galactosidase in live bacteria cells was achieved by confining fluorescent molecules produced by enzymatic activity within 100-pl chambers (Cai *et al.*, 2006). A glass microfluidic cell was an essential component of a new type of single-molecule trapping system where the Brownian motion of an individual fluorescent molecule is cancelled electrokinetically (Cohen and Moerner, 2006). Measurement of protein folding kinetics based on single-molecule FRET efficiency was performed using a microfabricated rapid mixer (Lipman *et al.*, 2003).

Electrophoretic separation of biomolecules by their charges and sizes can be integrated into a microfluidic device by implementing structures for injection plug formation and capillary-like microchannels (Wu *et al.*, 2004). Although microchip electrophoresis is a highly efficient separation technique, the conventional detection methods, which are based on optical or electrical signals only, do not provide a means to "identify" separated chemical species unless known standard samples are used for spiking. In the case of heterogeneous biological systems in dynamic equilibrium, where molecules bind weakly with each other, it is almost impossible to prepare a pure sample for identification purposes. We overcome this limitation by employing fluorescence fluctuation spectroscopy to extract molecular parameters of separated species. We regard the ability to characterize individual molecular behavior as one of the key advantages of single-molecule spectroscopy as opposed to the study of ensemble averages.

More specifically, we combine a microfluidic separation based on a two-component detergent mixture containing charged micelles with correlation analysis of laser-induced fluorescence signals as a detection modality. In this chapter, optimized protocols for the application of this technique to a model immunocomplex system and the experimental results are described. We suggest that this approach is a general one and can be used in many other situations to advantage.

It is necessary to mention that a similar but distinct approach using fluorescence correlation spectroscopy (FCS) for biomolecular analysis in continuous flow capillary electrophoresis (CE) system has been developed (Fogarty and Van Orden, 2009; Van Orden and Keller, 1998). Also, the use of photon counting histograms to study a protein charge ladder caused by different numbers of incorporated fluorescent probes has been reported previously (Kim *et al.*, 2007).

2. Microchip Fabrication

A microfluidic device for simple CE with a capture valve can be constructed using a multilayer soft lithography technique (Anderson *et al.*, 2000; Unger *et al.*, 2000). The fabrication procedures are divided into three steps: design drawing and mask printing, making a photoresist master on a silicon wafer, and making poly(dimethylsiloxane) (PDMS) channel structures using a master molding technique. In the following paragraphs, an optimized protocol for the fabrication of a CE chip is described.

2.1. Design drawing and photomask printing

Each layer of the microfluidic device is drawn electronically using vector graphics software. Macromedia FreeHand® 10 was used for the work presented, but more advanced versions of computer programs such as Adobe Illustrator® or Audodesk AutoCAD® can be used as well. One microchip is designed to fit into a 24 mm × 60 mm glass coverslip, as shown in Fig. 7.1. The standard 4-in. wafer can accommodate three such CE chips. At the final stage of design drawing, the objects that will be made with "negative" photoresists in the photolithography step should be converted into their "negative" images. In Fig. 7.1, the valve layer (shown in gray), which will be made with the SU-8 negative photoresist, requires such conversion.

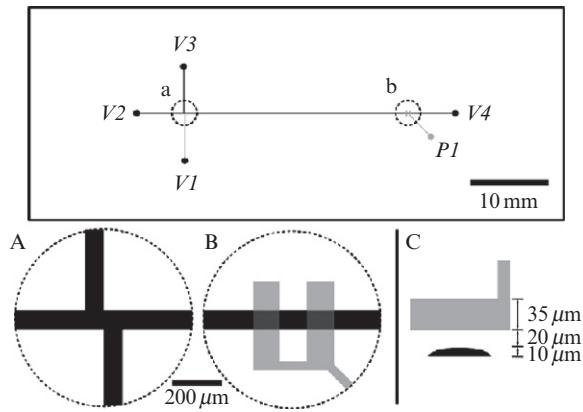

Figure 7.1 Drawing of a CE microchip with a capture valve: (A) the "double-T" region for injection plug formation; (B) region for capturing separated chemical species, where the distance from the double-T region to the capture region is 25 mm; and (C) the side-view of the capture region. There is a 20-μm thick PDMS membrane between the channel layer (black) and the valve layer (gray), which can be deformed pneumatically. *V1–V4* stand for access ports for the channel layer where high-voltage electrodes are inserted. *P1* is the access port for the valve layer where pressure for valve actuation is applied.

The finished design is printed on a transparency film, using a high-resolution photoplotter (32,512 DPI; Fineline Imaging, Colorado Springs, CO), which can achieve about 10-μm resolution. In case a photomask with a higher resolution is necessary, a chrome mask can be prepared at a higher cost either from an academic nanofabrication facility or from a commercial vendor equipped with a mask writer. It is capable of providing a resolution of features of about 1 μm if created with laser writing.

2.2. Molding master fabrication

A polymeric layer of well-defined thickness and shape can be created on a silicon wafer, using photolithography. The standard photolithography procedure consists of three steps: spin-coating, exposure, and developing. In spin-coating, the viscosity of the photoresist and the spin speed are adjusted to control the thickness of the structure. In exposure, the photoresist layer is exposed to ultraviolet (UV) light that is patterned by the photomask. Photoresists can be categorized into two groups according to their responses to this UV irradiation. A positive photoresist becomes soluble upon exposure, whereas a negative photoresist becomes insoluble upon exposure. In developing, the soluble portion of the photoresist is dissolved by a solvent called "developer," leaving the desired microstructure on the wafer surface. The protocol described here is optimized for creating a rounded channel structure, using SPR 220-7 positive photoresist (Shipley).

1. SPR 220-7 is spin-coated (3500 rpm, 40 s) on a 4-in. silicon wafer and prebaked at 90 °C for 200 s to form a 7-μm thick layer.
2. The photoresist layer is exposed to UV light (365 nm) for 15 s, using the exposure instrument protocol (Karl Suss, Waterbury Center, VT). No postexposure bake is necessary.
3. The exposed layer is developed for 270 s with LDD26W developer (Rohm and Haas, Marlborough, MA).
4. The wafer is postbaked at 120 °C for 10 min to reflow and transform the photoresist structure into a round shape. This step is critical to complete valve closure (Melin and Quake, 2007).
5. The photoresist master is inspected on a microscope to check its quality. Finally, the master mold is coated with perfluoro-1,1,2,2-tetrahydrooctyl-trichlorosilane (United Chemical Technologies, Bristol, PA) by exposing it to vapor in a vacuum desiccator to prevent adhesion of PDMS onto the master surface. Specifically, one drop of silane liquid is placed in a separate container inside the desiccator together with the silicon wafer.

2.3. Fabrication of PDMS chip

We use the following protocol to create multilayer channel structures in a PDMS device:

1. PDMS prepolymers (RTV 615A and 615B; GE Silicones, Waterford, NY) are mixed in a 5:1 mass ratio, poured onto the master for valve layer, degassed under vacuum, and cured at 80 °C for 1–2 h.
2. The PDMS slab is cut out with a scalpel, and holes for fluid access are punched with a syringe needle ground flat at the tip. Finished pieces are scotch-taped on both sides to prevent contamination.
3. PDMS prepolymers, mixed in a 20:1 mass ratio, is spin-coated on the master for making the channel layer, with the initial spin speed of 300 rpm for 9 s and the final spin speed of 3000 rpm for 45 s. The PDMS-coated wafer is placed on a flat surface at room temperature for 5 min to let the coating flow and flatten further. Then, the PDMS coating is cured at 80 °C for 20 min.
4. The 5:1 PDMS slab prepared in Step 2 is placed on the 20:1 PDMS-coated wafer and aligned by inspecting through a stereoscope. This alignment procedure can be repeated many times to achieve perfect spatial match because both pieces are fully cured. After alignment, gentle pressure is applied to seal completely the edges of the bonded pieces.
5. A 10:1 PDMS mix is poured around the aligned slabs, degassed, and cured at 80 °C for 1 h.
6. Chips are cut out with a scalpel, and access holes are punched in the same way as described in Step 2.
7. Glass coverslips (No. 1 1/2; VWR International, West Chester, PA) are spin-coated with a diluted 5:1 PDMS mix at an initial spin speed of 1000 rpm for 9 s and a final spin speed of 2000 rpm for 30 s. The diluted PDMS mix is prepared by adding 20 g of cyclohexane (179191; Sigma-Aldrich) to 10 g of the 5:1 PDMS mix. The coated coverslips are cured at 80 °C for 20 min.
8. The chips prepared in Step 6 are placed on the spin-coated coverslips and sealed with gentle pressure. The chips are placed in an 80 °C oven overnight for final bonding.
9. The chips are inspected on a microscope for defects and tested for valve functions (complete valve closure at a designated pressure value).

These chips can be stored for an extended period of time under a dry condition, at least for 3 months from our experience. When exposed to buffers and/or detergents, the surface property of PDMS usually changes and degrades over time. The quality of a microchip CE deteriorates after continuous usage of the chip for 8–10 h.

3. Instrumentation for Fluorescence Detection

The laser-induced fluorescence detection is achieved by using the following optical setup. A 532 nm laser beam (Compass 215M; Coherent Inc., Santa Clara, CA) or a 638 nm laser beam (RCL-025-638; Crystalaser,

Reno, NV), guided by a single-mode optical fiber (OZ Optics, Canada) and collimated with a 5× objective lens (Zeiss), is sent to an inverted microscope (TE300; Nikon, Melville, NY) as an excitation source for epi-illumination of the sample. The laser beam is reflected by a dichroic mirror (540DRLP or 400-535-635TBDR; Omega Optical, Brattleboro, VT) and focused by a high numerical aperture (NA) objective (Plan Apo, 60×, NA 1.20; Nikon). The resulting fluorescence photons are collected by the same objective lens, passed through the same dichroic mirror, a 50-μm pinhole, and a band-pass filter (595AF60, Omega Optical; HQ675/50m, Chroma Technology), and detected by an avalanche photodiode (SPCM AQR15; EG&G, Canada) (Fig. 7.2). The fluorescence signals are recorded with a counter/timer data acquisition card (PCI-6602; National Instruments, Austin, TX) and displayed as a signal–time graph on a computer screen, using a LabView® program. This real-time display of fluorescence intensity can be used for fine tuning the alignment of the optical components by adjusting them to maximize the fluorescence signal. Autocorrelation functions of the fluorescence signals are calculated by transferring the signals to a hardware digital correlator (Flex99R-480; Correlator.com, Bridgewater, NJ). The obtained correlation curves are fitted with IGOR Pro software (WaveMetrics, Inc., Portland, OR).

4. Detergent-Assisted Microchannel Electrophoresis

Capillary electrophoresis is a powerful separation technique utilizing the differences in ionic mobilities through a capillary under the action of an applied electric field (Jorgenson and Lukacs, 1983; St. Claire, 1996).

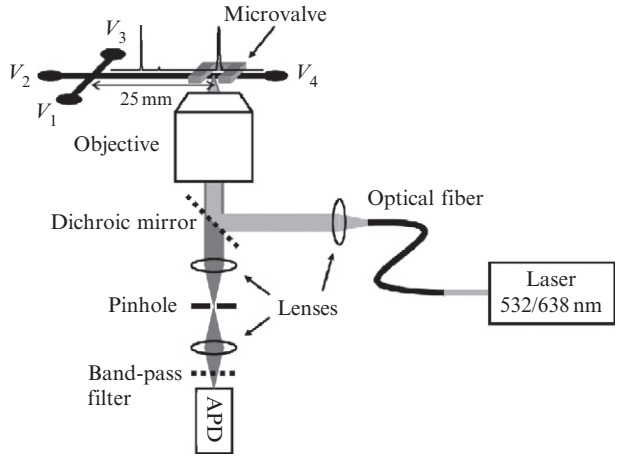

Figure 7.2 Optical setup for laser-induced fluorescence detection: APD, avalanche photodiode; V_i, the voltage applied to electrode i. Reproduced from Kim *et al.* (2007) by permission of The Royal Society of Chemistry.

A similar structure having separation resolution can be easily integrated into a microfluidic device, enabling electrophoresis experiment on a PDMS microchip. The native PDMS surface, however, is not suitable for electrophoretic separation of biomolecules because (1) the electroosmotic flow is not stable owing to uneven surface charge density and (2) the analytes can be easily adsorbed onto the hydrophobic PDMS surface, contributing to significant loss of analytes and the tailing of peaks during electrophoresis.

One remedy to this problem is to passivate the PDMS surface with detergent molecules. We developed a dynamic coating method using a mixture of a nonionic detergent (dodecyl maltoside, DDM) and an anionic detergent (sodium dodecyl sulfate, SDS) (Huang *et al.*, 2007). This procedure allows not only nearly complete rejection of adsorption of organic dye and protein molecules but also control of both electroosmotic flow and separation efficiency by varying the relative concentration of SDS, creating an environment similar to micellar electrokinetic chromatography (MEKC), where the presence of micelles promotes further separation of analytes (Terabe *et al.*, 1984). This surfactant system has been successfully applied to the separation of simple organic dyes, protein charge ladders, phycobiliproteins, and immunocomplexes. Detailed procedures for performing microchip CE experiments to separate the immunocomplexes between dye-labeled bovine serum albumin (BSA) and monoclonal antibody (mAb) are described below.

4.1. Preparation of separation buffer and sample solutions

The separation buffer contains 20 m*M* HEPES, pH 7.5, 0.1% (w/v) *n*-dodecyl-*β*-D-maltoside (Anatrace, Inc., Maumee, OH), and 0.01% (w/v) SDS (Sigma-Aldrich). For simple dye mixtures, 100 μM stock solutions of Alexa Fluor 647 succinimidyl ester (A20006; Invitrogen) and Cy5 succinimidyl ester (GE Healthcare, Piscataway, NJ) are prepared in the separation buffer and diluted to obtain desired concentrations. For immunocomplexes, 0.09 mg/ml BSA tetramethylrhodamine conjugate (A23016; Invitrogen) is prepared using the separation buffer; varying amounts (1.4, 0.20, and 0.028 mg/ml) of monoclonal anti-BSA antibody (B2901; Sigma) are added and incubated at least for 1 h. The immunocomplex solutions are then diluted to achieve concentrations in a nanomolar range after electrophoresis and capture, which enables FCS measurement with a good signal-to-noise ratio and resolvability.

The optimal composition of DDM and SDS in the separation buffer is sample-dependent. Therefore, a calibration experiment at an early stage will be necessary for different types of analytes.

4.2. Microchip electrophoresis with electrokinetic injection

1. One microliter of 1% (w/v) SDS solution is added to the bottom of each of the access ports, *V1*–*V3*, using a gel-loading pipet tip. The microchannels should be spontaneously filled with the solution via capillary

action. Then, the SDS solution is removed, which will not affect the capillary action because the volume necessary to fill the entire microchannel is negligibly small (22 nl), and 200 μl of the separation buffer is added to each of the access ports, *V1–V3*. After it is visually confirmed with a microscope that the liquid front reaches the access port *V4*, 200 μl of the separation buffer is added to *V4*. Whenever solution is added to the access ports, the formation of air bubbles at the bottom of the reservoirs should be carefully avoided to maintain electrical connection.

2. Voltages are applied (*V1–V3* = 1 kV, *V4* = 0 V) and the through-the-channel current is measured. The current will gradually decrease and stabilize at a value between 0.5 and 1 μA as 1% (w/v) SDS solution is replaced electrokinetically by the separation buffer. The electrical connection for all the three input ports (*V1–V3*) should be tested individually by monitoring electrical current; for example, the voltage setting *V1* = 1 kV, *V2–V4* = 0 V can be used to check the *V1* port. If an input port is found to have "zero" current, the air bubble at the bottom of that port should be removed by suction with a gel-loading pipet tip.
3. The objective lens is moved to the detection point, which is 25 mm away from the double-T region. The excitation laser is focused at the half height of the channel by monitoring the shape of the reflected beam. At this point, the fluorescence intensity obtained from the avalanche photodiode should be close to the background level, which is usually below 3000 photons/s (i.e., 3 kHz as in Fig. 7.3) in our optical setup.
4. The sample solution to be separated is added to *V1*. Voltages for electrokinetic injection (*V1* = 1 kV, *V2* = 700 V, *V3* = 0 V, *V4* = 700 V) are applied for 17 s. Then, voltages for electrophoretic separation (*V1* = 700 V, *V2* = 1 kV, *V3* = 700 V, *V4* = 0 V) are applied and

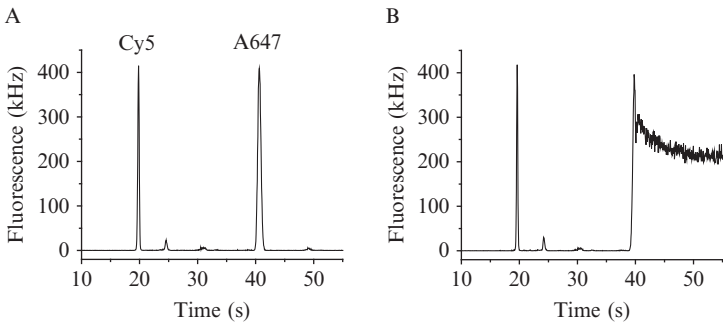

Figure 7.3 Separation and capture of a dye mixture: (A) electropherogram of the mixture of Cy5 and Alexa Fluor 647 (A647); (B) fluorescence signal after capturing the A647 peak. Once captured, the intensity drops because of diffusive mixing. Fluctuations caused by molecular diffusion can be observed. Reproduced from Kim *et al.* (2007) by permission of The Royal Society of Chemistry.

the fluorescence signal acquisition is initiated simultaneously. Synchronized operation of the high-voltage power supply and the photodetector is critical to obtaining reproducible results. This process should be repeated for each sample at least three times to ensure that no systematic error in migration time is observed. It should be noted that the separation result from the first run with a new sample added to the chip is usually not reliable because of disturbed injection profiles.

5. The migration times of separated peaks, which are determined in the previous step, can be used to capture a peak of interest. The same voltage settings are used for injection and separation except that the separation voltages are applied only for a specified period of time (i.e., the migration time of the peak to be captured). Immediately after turning off separation voltages, pressure is applied to the *P1* port to actuate the capture valves. The duration for applying separation voltages needs to be optimized depending on how fast the microvalves respond. When this scheme is used, a timing accuracy of 100 ms or better is sufficient for successful capture.

5. Fluorescence Correlation Spectroscopy

The separated peaks can be captured with microvalves and analyzed further by measuring molecular parameters based on fluorescence fluctuation signals. Here, we demonstrate the use of FCS for obtaining the diffusion coefficients of the immunocomplex species to determine the identities of the peaks.

In FCS experiments, fluctuations of the fluorescence intensity from the molecules that are passing through the focus of a laser beam are analyzed by calculating the autocorrelation function of the signal. The autocorrelation function $G(\tau)$, which contains information on the physical processes responsible for the fluctuations, is defined by

$$G(\tau) = \frac{\langle \delta I(t) \cdot \delta I(t+\tau) \rangle}{\langle I(t) \rangle^2} \tag{7.1}$$

where $I(t)$ is the fluorescence intensity at a time point t and $\delta I(t) = I(t) - \langle I(t) \rangle$, that is, the deviation of the signal from the ensemble average value $\langle I(t) \rangle$.

The main contributor to this fluctuation is molecular diffusion. When the molecule or the particle of interest is assumed to be freely diffusing and have constant fluorescence intensity, the autocorrelation function of that fluorescent species takes the form

$$G(\tau) = \frac{1}{\bar{N}}\left(1 + \frac{\tau}{\tau_D}\right)^{-1}\left(1 + \frac{\tau}{\kappa^2\tau_D}\right)^{-1/2} \tag{7.2}$$

where $\bar{N}$ is the average number of molecules in the observation volume, τ_D is the diffusion time, and κ is the geometry factor describing the shape of the observation volume. Both $\bar{N}$ and τ_D can be obtained by fitting the experimentally determined autocorrelation function with this equation.

The size of diffusing molecules can be estimated from the Stokes–Einstein relation:

$$D = \frac{k_B T}{6\pi\eta r} \tag{7.3}$$

where D is the diffusion coefficient, k_B is the Boltzmann constant, T is the absolute temperature, η is the viscosity of the medium, and r is the hydrodynamic radius of a spherical particle. This equation can be converted into a simple relation between r and τ_D in the following way.

The focal spot size (ω_0) is determined by obtaining FCS curves from dilution series of standard Alexa Fluor 594 solutions (Perroud *et al.*, 2005). The effective focal volume, V_{eff}, which is calculated from a plot of $\bar{N}$ versus concentration, is related to the spot size as $V_{eff} = \pi^{3/2}\kappa w_0^3$. After replacing D with an expression containing τ_D ($w_0^2 = 4D\cdot\tau_D$, where $\omega_0 = 0.32 \pm 0.05\,\mu$m) and inserting numerical values for constants ($k_B = 1.38 \times 10^{-23}$ J/(mol K)[1]; $T = 298.15$ K; $\eta = 9.46 \times 10^{-4}$ Pa s), a simple relation is obtained:

$$r = 9.46 \times 10^{-6}\tau_D \tag{7.4}$$

Finally, assuming spherical shapes for immunocomplexes, the molecular weight of a protein complex is found to be proportional to the cube of the diffusion time obtained from FCS measurements.

For a mixture of Cy5 and A647 fluorophores (Fig. 7.3), the FCS measurements performed on a microchip after CE and capture are compared with those obtained individually using a standard solution chamber. As summarized in Table 7.1, the diffusion times measured within a 50-pl capture region are consistent with the results obtained in a 50-μl sample chamber. It needs to be noted that resolving Cy5 and A647 purely based on fitting with a multiple-species diffusion model will be more difficult and less accurate because the diffusion times of these fluorophores are very similar.

Figure 7.4 shows the separation results of the immunocomplexes between bovine serum albumin labeled with tetramethylrhodamine (TMR-BSA) and monoclonal anti-BSA antibody (mAb), using the DDM/SDS micellar system on a standard double-T CE chip. The observed numbers of separated peaks and the changes in their relative abundances are in agreement with the previous experimental results obtained with an

acid-modified CE microchip (Luo *et al.*, 2006). The dependence of relative peak heights on the mAb concentration suggests that different peaks correspond to protein complexes formed at different stoichiometries.

Table 7.1 FCS parameters obtained for simple dye solutions

	Individual dye in a glass-bottom chamber		1:1 mixture separated in a microchip	
	Cy5	A647	Cy5	A647
τ_D (μs)	128 ($\pm$4)	137 ($\pm$3)	125 ($\pm$3)	138 ($\pm$2)
$\bar{N}$	5.16 ($\pm$0.06)	5.62 ($\pm$0.03)	3.7 ($\pm$0.4)	3.7 ($\pm$0.3)

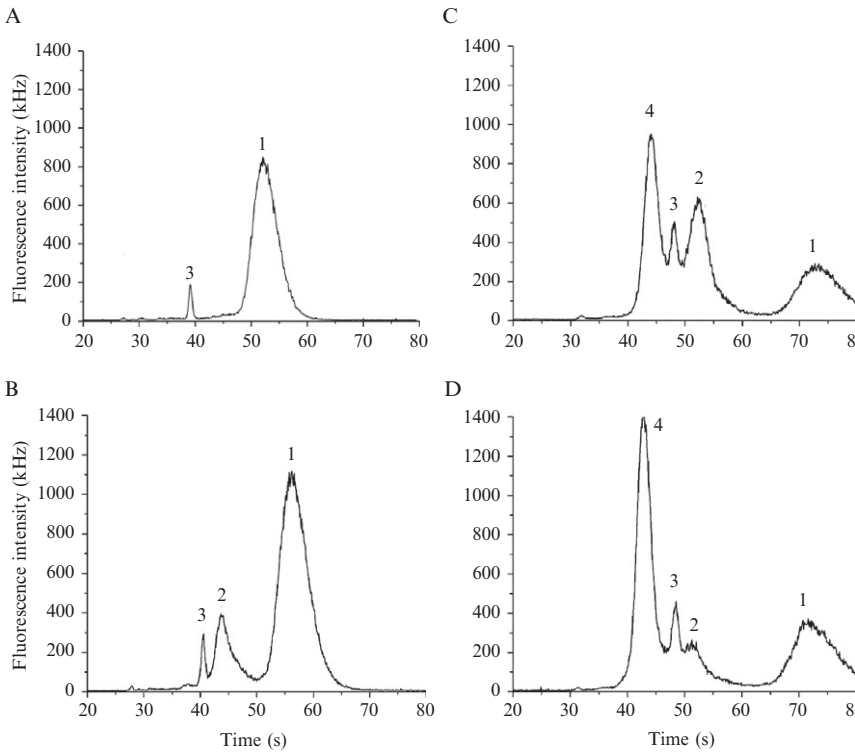

Figure 7.4 The electropherograms for the immunocomplexes between TMR-labeled BSA and anti-BSA antibody. A solution containing 0.09 mg/ml TMR-BSA was supplemented with (A) 0 mg/ml, (B) 0.028 mg/ml, (C) 0.20 mg/ml, and (D) 1.4 mg/ml of anti-BSA antibodies. Peak 3 is thought to be free TMR from incomplete purification of the fluorescently labeled protein sample. The variation in migration times arises from different concentrations of electrolytes in the immunocomplex mixtures, which are made from antibody solutions containing salts.

We consider two possibilities for immunocomplex formation. If the antigen (i.e., BSA) has more than one recognition site, the order of formation of immunocomplexes upon increasing the antibody concentration will be BSA, BSA-mAb, and BSA-mAb_2 (Fig. 7.5A). In contrast, if the antibody has multivalency, which is reasonable recalling the T-shaped structure of the Fab fragments of the antibody (Harris *et al.*, 1992), the order of formation upon the addition of antibody will be BSA, BSA_2-mAb, and BSA-mAb (Fig. 7.5B). Since the molecular weights of BSA and mAb are known (~69 and ~150 kDa, respectively), the expected diffusion times can be calculated. Figure 7.5 shows these two scenarios schematically and tabulates the expected FCS parameters, assuming that the immunocomplexes are spherical in shape and the densities of the proteins are constant.

The experimental results agree with the second hypothesis (Fig. 7.5B), as summarized in Table 7.2. When the mixture contains TMR-BSA only, the electropherogram has two peaks (Fig. 7.4A). The stronger and broader peak (Peak 1), which is TMR-BSA, yields the diffusion time of 469 ± 20 μs. The other peak (Peak 3), smaller and sharper, is composed of TMR impurities, which is evident from its shorter diffusion time (116 ± 5 μs) and it is present in all four samples at nearly the same concentration. As the concentration of mAb increases, another peak (Peak 2) starts to appear

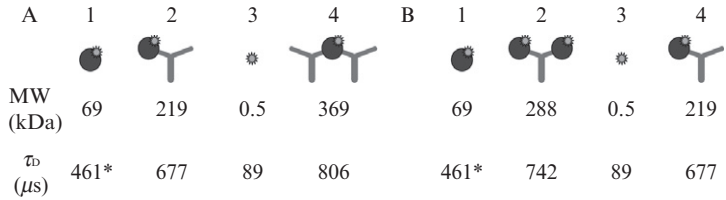

Figure 7.5 Expected diffusion times of immunocomplexes based on two different assembly hypotheses. (A) Multivalency of the antigen is assumed. (B) Multivalency of the antibody is assumed. The diffusion time of TMR-BSA is estimated to be 461 μs, an average value calculated from three FCS measurements.

Table 7.2 FCS parameters obtained from immunocomplexes separated by microchip CE

Mixture in Fig. 7.4	TMR-BSA (mg/ml)	mAb (mg/ml)	Peak 1	Peak 2	Peak 3	Peak 4
(A)	0.09	0	469 ± 20	–	116 ± 5	–
(B)	0.09	0.028	483 ± 18	849 ± 32	–	–
(C)	0.09	0.20	–	858 ± 25	–	770 ± 44
(D)	0.09	1.4	432 ± 19	–	–	718 ± 11

between these two peaks at about a 44-s migration time (Fig. 7.4B) and is found to have a diffusion time longer than that of TMR-BSA (849 ± 32 μs). At even higher mAb concentrations, another peak (Peak 4) appears at the shortest migration time with a diffusion time of 770 ± 44 and 718 ± 11 μs (Fig. 7.4C and D, respectively). The observation that the values of the diffusion times of the chemical species in Peak 2 are larger than those of Peak 4 is consistent with the ''multivalent antibody'' hypothesis. The discrepancy between the calculated diffusion times and the measured values is partly because (1) the immunocomplexes have nonspherical shapes and (2) the resolved peaks are still overlapping, arising from incomplete separation. We note that the difference in diffusion times of these complexes is not significant and, therefore, the approach of fitting the FCS data with a multiple-species model (i.e., without electrophoretic separation) will produce larger errors in determining diffusion times and relative abundances of distinct molecular aggregates. Once again, the advantages are apparent of being able to carry out single-molecule spectroscopy.

ACKNOWLEDGMENTS

We thank Yiqi Luo for helping with the preparation of immunocomplex solutions. S. K. acknowledges the Stanford Bio-X Graduate Fellowships. This work was supported by the National Science Foundation under MCB-0636284 and MCB-0749638.

REFERENCES

Anderson, J. R., Chiu, D. T., Jackman, R. J., Cherniavskaya, O., McDonald, J. C., Wu, H. K., Whitesides, S. H., and Whitesides, G. M. (2000). Fabrication of topologically complex three-dimensional microfluidic systems in PDMS by rapid prototyping. *Anal. Chem.* **72,** 3158–3164.

Cai, L., Friedman, N., and Xie, X. S. (2006). Stochastic protein expression in individual cells at the single molecule level. *Nature* **440,** 358–362.

Cohen, A. E., and Moerner, W. E. (2006). Suppressing Brownian motion of individual biomolecules in solution. *Proc. Natl. Acad. Sci. USA* **103,** 4362–4365.

Cui, B. X., Wu, C. B., Chen, L., Ramirez, A., Bearer, E. L., Li, W. P., Mobley, W. C., and Chu, S. (2007). One at a time, live tracking of NGF axonal transport using quantum dots. *Proc. Natl. Acad. Sci. USA* **104,** 13666–13671.

Fogarty, K., and Van Orden, A. (2009). Fluorescence correlation spectroscopy for ultrasensitive DNA analysis in continuous flow capillary electrophoresis. *Methods* **47,** 151–158.

Harris, L. J., Larson, S. B., Hasel, K. W., Day, J., Greenwood, A., and Mcpherson, A. (1992). The 3-dimensional structure of an intact monoclonal-antibody for canine lymphoma. *Nature* **360,** 369–372.

Huang, B., Kim, S., Wu, H., and Zare, R. N. (2007). Use of a mixture of n-dodecyl-beta-D-maltoside and sodium dodecyl sulfate in poly(dimethylsiloxane) microchips to suppress adhesion and promote separation of proteins. *Anal. Chem.* **79,** 9145–9149.

Jorgenson, J. W., and Lukacs, K. D. (1983). Capillary zone electrophoresis. *Science* **222,** 266–272.

Kim, S., Huang, B., and Zare, R. N. (2007). Microfluidic separation and capture of analytes for single-molecule spectroscopy. *Lab Chip* **7,** 1663–1665.

Lipman, E. A., Schuler, B., Bakajin, O., and Eaton, W. A. (2003). Single-molecule measurement of protein folding kinetics. *Science* **301,** 1233–1235.

Luo, Y., Huang, B., Wu, H., and Zare, R. N. (2006). Controlling electroosmotic flow in poly(dimethylsiloxane) separation channels by means of prepolymer additives. *Anal. Chem.* **78,** 4588–4592.

Melin, J., and Quake, S. R. (2007). Microfluidic large-scale integration: The evolution of design rules for biological automation. *Annu. Rev. Biophys. Biomol. Struct.* **36,** 213–231.

Perroud, T. D., Huang, B., and Zare, R. N. (2005). Effect of bin time on the photon counting histogram for one-photon excitation. *ChemPhysChem* **6,** 905–912.

St. Claire, R. L. (1996). Capillary electrophoresis. *Anal. Chem.* **68,** R569–R586.

Terabe, S., Otsuka, K., Ichikawa, K., Tsuchiya, A., and Ando, T. (1984). Electrokinetic separations with micellar solutions and open-tubular capillaries. *Anal. Chem.* **56,** 111–113.

Unger, M. A., Chou, H. P., Thorsen, T., Scherer, A., and Quake, S. R. (2000). Monolithic microfabricated valves and pumps by multilayer soft lithography. *Science* **288,** 113–116.

Van Orden, A., and Keller, R. A. (1998). Fluorescence correlation spectroscopy for rapid multicomponent analysis in a capillary electrophoresis system. *Anal. Chem.* **70,** 4463–4471.

Wu, H., Wheeler, A., and Zare, R. N. (2004). Chemical cytometry on a picoliter-scale integrated microfluidic chip. *Proc. Natl. Acad. Sci. USA* **101,** 12809–12813.